Appl. Sci. Converg. Technol. 29(6): 167-169 (2020)
https://doi.org/10.5757/ASCT.2020.29.6.167
eISSN : 2288-6559

Research Paper Check for updates

Non-Maxwellian Electron Energy Probability Functions in an Indirectly Heated Cathode Bernas Source

Received September 28, 2020; revised November 4, 2020; accepted November 4, 2020

June Young Kim[a], Won Ik Jeong[a], M.A.I. Elgarhy[a,b], Jaeyoung Choi[a], Geunwoo Go[a], Kyoung-Jae Chung[a,*], and Yong-Seok Hwang[b,*]

[a]Department of Nuclear Engineering, Seoul National University, Seoul 08826, Republic of Korea
[b]Physics Department, Faculty of Science, Al-Azhar University, Cairo 11884, Egypt

*Corresponding author E-mail: jkjlsh1@snu.ac.kr, kyoungjae.chung@gmail.com, yhwang@snu.ac.kr

ABSTRACT

The indirectly heated cathode (IHC) Bernas source is used in plasma process devices as it can produce a high current of desired ion species. The formation of various ion species is associated with the complex electron production mechanism inside the source, including beam–plasma interaction and energy relaxation. However, plasma diagnostics inside IHC sources has been limited by the assumption of a Maxwellian distribution. In this work, the discharge characteristics of IHC plasmas were investigated by analyzing the electron energy probability functions (EEPFs) under various conditions. The shape of the EEPF is dominantly affected by the voltage applied to the hot-cathode and repeller (i.e., cathode voltage), whereby the kinetic energy of the beam electrons is determined. With increasing cathode voltage, the EEPFs show a bi-Maxwellian-like distribution with the bulk and energetic electron groups. The thermalization among the two electron groups with increasing magnetic field makes the EEPFs to follow a Maxwellian distribution. The absolute value of the density and effective temperature of the electron are mainly governed by the bulk electron group with a relatively higher density, and the changes in the electric potentials are explained in the context of the confinement of the energetic electrons.

Keywords: Indirectly heated cathode Bernas source, Non-Maxwellian energy distribution, Penning ionization source

1. Introduction

Over the past several decades, the Penning ionization gauge (PIG) has been used as an ion source as it can extract high-current ion beams [1,2]. The PIG source has advantages in determining the fraction and charged-state of ion species by controlling the energy of the electrons. These features have made the PIG source suitable for applications in semiconductor production and accelerators [1–4].

The characteristics of the ion beam are directly related to the discharge property of the source, and there are as many types of source structures as the long history of PIG sources. The most popular source type among PIG sources is the indirectly heated cathode (IHC) Bernas source [2]. Unlike conventional PIG structures, the IHC source not only has an improved life-time but also has an effective discharge mechanism represented by the confinement of the beam electrons under the electric field combined with the magnetic field [1,2,5,6].

The plasma discharge initiated by the beam electrons within the electric and magnetic fields exhibits various physical phenomena. Theoretical works have shown the evolution of the electron energy probability function (EEPF) through beam–plasma interaction and quasi-linear relaxation of the electrons, and experimental works have reported various physical phenomena related to beam–plasma interaction in laboratory-level linear devices [5,6]. However, despite the long history of the sources, authors studying IHC sources focused on finding the plasma discharge conditions that can improve the plasma process yield from an industrial aspect, with no detailed analysis of the electron energy distribution, thus limiting our understanding of the underlying physics in PIG sources.

In this study, the plasma property of an IHC source is investigated by measuring the EEPFs at the center of the device. The source is characterized by performing diagnostics under various voltages of the hot-cathode and repeller (i.e., cathode voltage) and magnetic field strength, which are the main control parameters of the plasma process.

2. Experimental setup

The IHC source used in this study has two cathodes (hot-cathode and repeller) with a radius of 8 mm [Fig. 1]. The emitted thermal electrons from the hot-cathode are accelerated by the cathode sheath and are confined by the axial magnetic field and sheaths formed at both the cathode and repeller. Subsequently, the beam electrons collide with the argon neutral particles in the IHC sources.

A magnetic field is created by a Helmholtz coil placed symmetrically along the source axis. The Helmholtz coil–pair with 310 turns provides a uniform magnetic field at the center of the source within 1 sigma (1.85 %). The base pressure in the IHC source is maintained below 5×10^{-6} Torr. Argon gas, controlled using a mass flow meter, is used in this experiment.

The plasma parameters at the center of the discharge chamber are measured using a single Langmuir probe with a tungsten wire (1

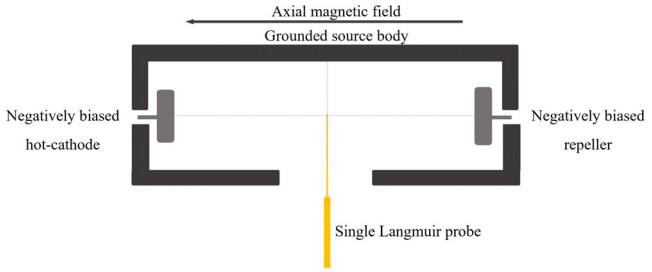

Figure 1. Cut-away view of the indirectly heated cathode Bernas source. A single Langmuir probe is located at both the radial and axial centers.

mm in length and 0.15 mm in radius). The influence of the magnetic field on the probe diagnostics is negligible because the effective probe radius (0.15 mm) is smaller than the electron gyro radius (~0.9 mm) [7]. The working pressure inside the source is 1.3 mTorr with an argon flow rate of 2.3 sccm. Since the area of the probe body is only 0.25 % of the inner area of the IHC source, probe perturbation on the measurement is negligible when the surface loss is the dominant loss channel.

The electron energy distribution functions (EEDFs) are obtained by calculating the second derivative of the measured current–voltage characteristic curve using the Druyvesteyn method without making any sheath assumptions regarding the energy distribution [7,8]. In this method, two assumptions should be satisfied: (1) The electrons in the plasma have an isotropic velocity distribution, (2) The plasma is collisionless at the relevant length scale (i.e., the probe diameter, probe holder diameter, and Debye length must be less than the electron mean free path). The second derivative $I_e''(\varepsilon)$ is proportional to the EEPF $f_e(\varepsilon)$, which is related to the EEDF g_e $(\varepsilon) = \varepsilon^{1/2} f_e(\varepsilon)$ as $g_e(\varepsilon) = 2m/e^2\ A(2\varepsilon/m_e)^{1/2} I_e''(\varepsilon)$, where m_e, e, ε, and A are the electron mass, elementary charge, electron energy in volts, and probe area, respectively. The electron density n_e and effective electron temperature T_{eff} corresponding to the mean electron energy are determined from the integral of the EEPF as [8]: $n_e(\varepsilon) = \int_0^\infty g_e(\varepsilon)d\varepsilon$, $T_{eff} = \int_0^\infty \varepsilon g_e(\varepsilon)d\varepsilon \,/\, \int_0^\infty g_e(\varepsilon)d\varepsilon$.

3. Results and Discussion

3.1. Cathode voltage effect

When a voltage higher than the electron/neutral impact ionization energy of argon gas (15.76 eV) is applied to the hot-cathode, discharge can occur. Accordingly, we observe changes in the plasma parameters by applying a cathode voltage ranging from 20 to 40 V at a magnetic field strength of 42 G. The most prominent change in the EEPFs accompanied by the variation in the cathode voltage is the bi-Maxwellianization [Fig. 2]. As the cathode voltage increases, the amount of high-energy tail of the EEPF is gradually increased. The energy range of the high-energy tail is directly related to the sheath potential of the hot-cathode. The sheath potential at the hot-cathode surface is determined by the summation of the plasma potential and the cathode voltage. Subsequently, the sheath potential determines the kinetic energy of the beam electrons at the initial stage of the discharge. These beam electrons produce secondary electrons as a result of the impact ionization process, and the energy exchange via electron-electron collisions with the secondary electrons produces thermalized

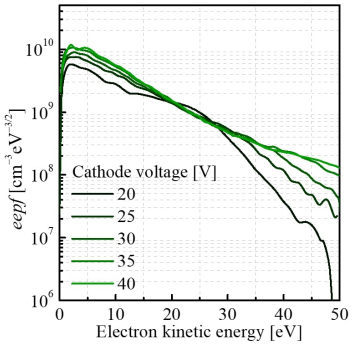

Figure 2. Change in the EEPFs at the radial center at different cathode voltages.

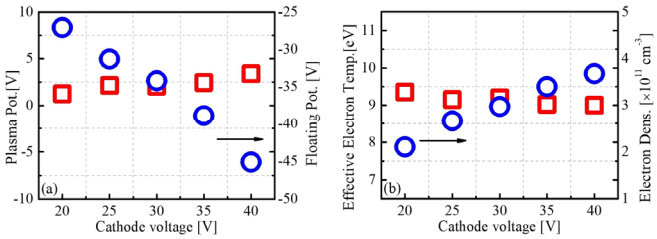

Figure 3. Changes in (a) the plasma and floating potentials and (b) the effective electron temperature and electron density at different cathode voltages.

bulk electrons. The beam electrons that have undergone beam–plasma interaction and energy relaxation form a high-energy tail of the EEPF [5,6]; these electrons are classified as the energetic electron group. Eventually, the EEPFs are classified into bulk electron and energetic electron groups based on the cathode voltage.

The electron density increases with the increase in the cathode voltage while the effective electron temperature is slightly decreased [Fig. 3(b)]. The changes in the bulk electron group in the EEPFs are responsible for the variation in the electron density and the effective electron temperature because they occupy a relatively large proportion; the slope of the EEPFs with an energy below the cathode voltage under each condition increases, indicating a decrease in the thermal energy of the bulk electron group. The plasma potential slightly increases with the increase in the cathode voltage, while the variation in the floating potential is prominent [Fig. 3(a)]. The slight increase in the plasma potential is considered be due to the increase in the number of energetic electrons (i.e., an increase in the plasma potential to suppress energetic electron losses by ambipolar diffusion). The floating potential shows a negative value because of the abundant energetic electrons; as the number of energetic electron group is increased, the floating potential shifts to a more negative value.

3.2. Magnetic field strength effect

In this section, we observe the changes in the plasma parameters with respect to the magnetic field variation at each cathode voltage. The cathode voltages are fixed at 25 and 40 V at which nearly Maxwellian and bi-Maxwellian-like EEPFs are observed, respectively. Subsequently, the evolution of the EEPF is analyzed by varying the magnetic field from 64 to 170 G at each cathode voltage.

At a low cathode voltage, the EEPF shows a Maxwellian distribution with a weak bump at a kinetic energy corresponding to the

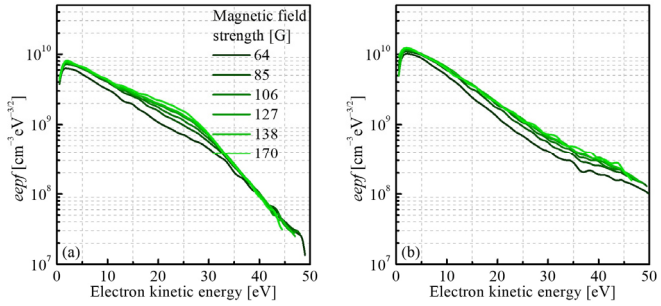

Figure 4. Changes in the EEPFs with the magnetic field strength ranging from 64 to 170 G at cathode voltages of (a) 25 V and (b) 40 V, respectively.

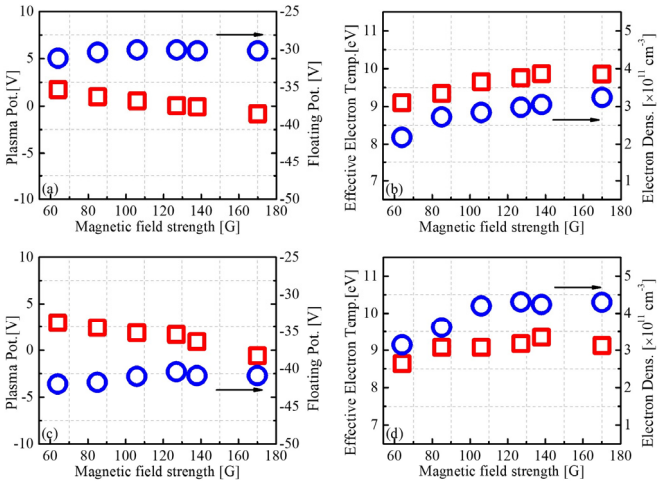

Figure 5. Changes in the plasma and floating potentials at different magnetic field strengths at cathode voltages of (a) 25 V and (c) 40 V, and the effective electron temperature and electron density at cathode voltages of (b) 25 V and (d) 40 V, respectively.

cathode voltage under a weak magnetic field strength, and the beam component disappears with increasing magnetic field [Fig. 4(a)]. To observe an evident EEPF evolution, the experimental data are fitted using the Maxwellian EEPF equation. At a magnetic field strength of 64 G, the electron temperature is 8.5 eV and increases to 14 eV at 170 G, implying an increased confinement of the energetic electrons. However, a depleted tail of the EEPFs at a high kinetic energy is clearly seen under high magnetic field strengths, and this is attributed to the increase in the electron impact ionization. When the cathode voltage is high (40 V), the EEPF shows a bi-Maxwellian-like distribution [Fig. 4(b)]. The changes in the electron temperature of the two electron groups (e.g., the bulk and energetic electrons) divided based on the cathode voltage are similar to the results obtained under low-cathode-voltage conditions. The temperature of the bulk electron group increases from 7 to 9 eV, while that of the energetic group decreases from 20 to 14 eV.

The absolute value of the floating potential slightly decreases and saturates with the increase in the intensity of the magnetic field under the two cathode voltage conditions [Figs. 5(a) and 5(c)]; this can be attributed to the cooling of the energetic electrons through a collisional loss under a high magnetic field strength (a slight increase in the slope of the EEPFs is seen). In the case of the plasma potential, the electron confinement in the local region causes a flux conservation effect through a reduction in the plasma potential.

Among the factors found in this basic characteristic study, the plasma potential can be mainly determined by the following mechanism: 1) Electron confinement in the local region (decreases the plasma potential) and 2) Increase in the number of energetic electrons (increases the plasma potential to suppress the loss of energetic electrons via trapping through ambipolar potential). Both the electron density and the effective electron temperature are determined by the tendency of the bulk electrons having relatively high proportion in the local region [Figs. 5(b) and 5(d)]. The reduction in the electron density variation is related to the saturation of the magnetic confinement by triggering the Simon-Hoh instability [9].

4. Conclusions

A plasma characterization of the IHC source is performed by analyzing the EEPFs under various discharge conditions. The shape of the EEPF is dominantly affected by the energetic electrons generated in the cathode sheath. The EEPFs exhibit a non-Maxwellian distribution with bulk and energetic electron groups. This shows that the characterization and modeling of the plasma parameters under various process conditions should not be performed under the assumption of thermally equilibrated electrons with a single temperature. In addition, it is emphasized that the confinement of the energetic electrons plays a leading role in this non-Maxwellian energy distribution, and their spatial distribution may be a key factor in setting the condition for the plasma process.

Acknowledgement

This research was supported by a Basic Science Research Program through the National Research Foundation of Korea (NRF) funded by the Ministry of Science, ICT & Future Planning (2020R1C1 C1009547), the NRF funded by the Korea government (MSIT) (2019 M2D1A1080261), and Korea research fellowship program (KRF) grant (2018H1D3A1A01074835).

References

[1] B. Wolf, Handbook of Ion Sources (CRC Press, 1995).
[2] I. G. Brown, The Physics and Technology of Ion Sources, 2nd Ed. (John Wiley & Sons, 2004).
[3] E. Heinicke and H. Baumann, Nucl. Instrum. Methods 74, 229 (1969).
[4] R. G. Wilson and G. R. Brewer, Ion beams: with applications to ion implantation, (1973).
[5] H. Schulte, B. H. Wolf, and H. Winter, IEEE Trans. Nucl. Sci. 23, 1053 (1976).
[6] Y. Sato, A. Kitagawa, H. Ogawa, and S. Yamada, J. Appl. Phys. 76, 3947 (1994).
[7] R. B. Lobbia and B. E. Beal, J. Propul. Power 33, 566 (2017).
[8] M. A. Lieberman and A. J. Lichtenberg, Principles of Plasma Discharges and Materials Processing (John Wiley & Sons, 2005).
[9] Y. Sakawa, C. Joshi, P. K. Kaw, F. F. Chen, and V. K. Y. Jain, Phys. Fluids B: Plasma Phys. 5, 1681 (1993).